The contribution of x-ray specular reflectometry to the oxygen-induced magnetic properties in Pt/Co/AlOx

Houmed Garad, Luc Ortega, Aline Y. Ramos, Jacques Marcus, Frédéric Gay, Farid Fettar, Stephane Auffret, Bernard Rodmacq, Bernard Dieny

The contribution of x-ray specular reflectometry to the oxygen-induced magnetic properties in Pt/Co/AlO$_x$

H. Garad,[1,a)] L. Ortega,[1] A. Y. Ramos,[1] J. Marcus,[1] F. Gay,[1] F. Fettar,[1] S. Auffret,[2] B. Rodmacq,[2] and B. Dieny[2]
[1]*Institut Néel, CNRS and Université Joseph Fourier, BP166, F-38042 Grenoble Cedex 9, France*
[2]*SPINTEC, UMR 8191 CEA-CNRS-UJF, 38054 Grenoble Cedex, France*

(Presented 16 November 2010; received 8 October 2010; accepted 16 December 2010; published online 6 April 2011)

Two key parameters were analyzed in Si/SiO/Pt/Co/AlO$_x$: the oxidation time of the Al layer resulting in AlO$_x$, and the *ex situ* annealing temperatures varied in the 15 and 55 s and 20, 300, and 450 °C ranges, respectively. For intermediate annealing temperatures (~300 °C), the quantitative analysis of specular reflectometry data shows that the progressive oxidation of layers by increasing the oxidation time goes along with an improvement of the homogeneity of the alumina layer. This outcome casts new light on the temperature dependence of magnetic properties of the samples. The remarkable temperature variation of the coercive field, extracted from extraordinary Hall effects in the 5–300 K range, is associated with structural change due to Co–oxygen bondings, which leads to strong pinning of Co spins in the low temperature regime. © *2011 American Institute of Physics*. [doi:10.1063/1.3563060]

In measured tunnel magnetoresistance ratios (TMR), the exact chemical composition along the different interfaces plays a very significant role as it determines the degree of polarizations (related to TMR) of the tunneling electrons.[1] In addition, the presence of specific layers for magnetic electrodes could induce a perpendicular magnetic anisotropy (PMA), which can be more promising than in-plane magnetic anisotropy.[2] More specifically in these kinds of nanostructures, a perpendicular magnetic tunnel junction implies two electrodes of ferromagnetic layers inserting an oxide one. Previous studies[3–5] reported a change of the magnetic anisotropy from in-plane to out-of-plane *at room temperature* (RT) for Si/SiO$_2$/Pt(3 nm)/Co(0.6 nm)/Al(1.6 nm) + t_{Ox} either for efficient oxidation times values (namely t_{Ox}), or by increasing the annealing temperature (namely T_{Ann}) of the trilayer. Such change seems to be related to the diffusion of the oxygen, induced by the annealing (via T_{Ann}) and/or the quantity of oxygen (via t_{Ox}), toward the Co/AlO$_x$ interface. In other words, the Co–Al bonds would be replaced by Co–O ones due to the annealing and/or the oxidation time.[4,6] However, the dependencies of the magnetic properties as a function of deposition parameters are not completely understood, especially at *low temperature*. Also, various structural schemes can be at the origin of improved PMA: oxygen at the interfaces between Co and AlO$_x$, Co–Pt intermixing, or chemical modification. The focus of this paper is to confront these hypotheses to quantitative results deduced from x-ray specular reflectometry (XRR). For two typical samples, one underoxidized and the other overoxidized, the strong temperature dependence of magnetic properties at low temperature is explained by chemical and structural characterizations of layers. In particular, the Co–oxygen bondings are mainly at the origin of the huge increase of coercive fields when the temperature is lowered.

In the present study we considered a low oxidation time ($t_{Ox} = 15$ s) and a high oxidation time ($t_{Ox} = 55$ s) corresponding, respectively, to a partial and a total oxidation of the Al layer. The details of the sample elaboration are given elsewhere.[5] The annealing temperatures are 300 and 450 °C and the as-deposited sample is considered as $T_{Ann} = 20$ °C in the remainder of the manuscript. The specular x-ray reflectometry measurements were carried out with a Bruker D8 Discover diffractometer using a line focus from a Cu target x-ray tube ($\lambda = 0.15418$ nm). The data were collected up to around 16° for 2θ reflection angles, corresponding to momentum transfer $Q_z = [4\pi/\lambda]\sin\theta$ of about 11.3 nm^{-1}. The transverse diffuse scans, permitting to estimate the topological roughness at interfaces, are not shown in that present manuscript. Only the interface width [called root mean square (rms) in the following], containing both the topological roughness and intermixing parameters between consecutive layers as developed in Ref. 7 (for Al transition-metal bilayers), will be considered and extracted from specular data. The forward diffuse scatter measured in an offset θ–2θ scan was systematically subtracted from the measured specular scatter. The quantitative analysis of XRR measurements is carried out using Bruker LEPTOS software.[8] The experimental scans are fitted with theoretical curves built using the standard Parratt algorithm[9] for appropriate models of stacks, and for 2θ ranging from 0.4° to 12°. Extraordinary Hall effects (EHE) were performed at 300 and 5 K, with an applied magnetic field H up to 8 T perpendicular to the film plane.

Figure 1 displays the whole set of XRR curves. For the two sets of data corresponding to the two oxidation times t_{Ox}, the higher the annealing temperature is, the narrower and more marked the XRR fringes are. This effect is stronger

a)Author to whom correspondence should be addressed. Electronic mail houmed.garad@grenoble.cnrs.fr.

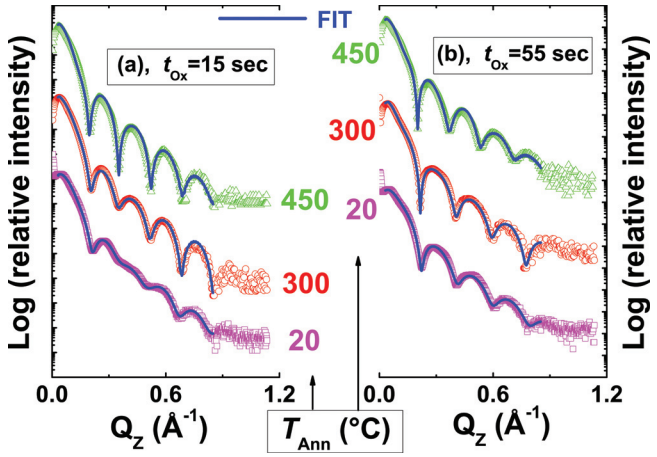

FIG. 1. (Color online) XRR data with fits (—) for as-grown (□) and annealed Pt/Co/AlO$_x$. The annealing temperature T_{Ann} is 300 °C (○), and 450 °C (Δ), and the oxidation time t_{Ox} is 15 s (a) and 55 s (b). The signals are shifted in the *y* direction.

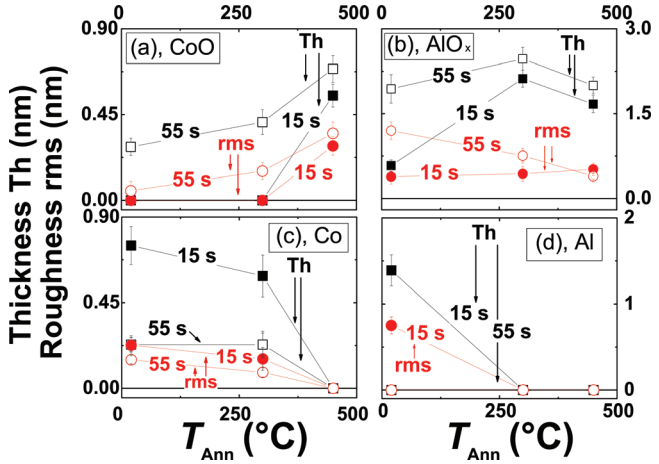

FIG. 2. (Color online) Thicknesses (Th) and roughness (rms) vs T_{Ann} for each layer [CoO (a), AlO$_x$ (b), Co (c), and Al (d)] of Pt/Co/AlO$_x$ oxidized during 15 s and 55 s (as noted in the curves).

for the low t_{Ox} [Fig. 1(a)] than for the high t_{Ox} [Fig. 1(b)]. Moreover, striking differences are noted between the two sets at low annealing temperature ($T_{Ann} = 20$ °C), whereas these differences vanish at higher T_{Ann}. These modifications in XRR data reveal change of the structure of stacks by varying as well t_{Ox} as T_{Ann}. Both previous parameters lead to the smoothing of the interfaces and improvement of the layers definition. More quantitatively, the construction of an appropriate stacking model for the layers is a critical point. First, we consider the sample with the lower oxidization (lower t_{Ox} and lower T_{Ann}). In this sample the only oxidized layer is the top layer Al. The architecture of the multilayer is Pt/Co/Al/AlO$_x$. The hypothesis that oxygen does not penetrate into buried layers (Co, Pt) is checked in this sample from previous x-ray spectroscopy measurements.[4] Taking into account the best set of parameters for t_{Ox} = 15 s as starting values, the procedure is iteratively repeated for the as-deposited sample with higher t_{Ox} (55 s). For more oxidized samples a CoO layer might be included in the stacking. The architecture for the multilayer in these samples is then Pt/Co/CoO/AlO$_x$. For each annealing temperature, the crossover between the two architectures occurs with the full oxidation of the Al layer for a certain oxidation time t^*_{Ox}. This crossover time can be determined precisely if samples with intermediate values of t_{Ox} are also considered. In the as-deposited series, the crossover oxidation time has been deduced at $t^*_{Ox} \approx 40$ s from a previous study.[6] Finally, to adjust XRR data for all annealed samples, the fitting procedure is repeated, with t^*_{Ox} properly estimated for each annealing temperature. For the samples annealed at 300 and 450 °C, $t^*_{Ox} = 0$ (no Al layers).

The fits are displayed in Figs. 1(a) and 1(b). For each fitted curve, three parameters are individually obtained for each layer of the stack: the thickness (Th), the roughness (rms), and the mass density (ρ). The evolutions of these parameters with the thermal annealing for both set of measurements are shown in Fig. 2 (for Th and rms) and Fig. 3 (for ρ). First, it remains an Al layer only for the as-grown samples oxidized during $t_{Ox} = 15$ s [Fig. 2(d)], and no Co layer is detected for $T_{Ann} = 450$ °C [Fig. 2(c)]. Second, the higher T_{Ann} is, the more CoO and Co thicknesses for both samples (15 and 55 s) increases and decreases, respectively [Figs. 2(a) and 2(c)]. At the same time, whereas Th(AlO$_x$) for $t_{Ox} = 15$ s quickly grows between 20 and 350 °C, Th(AlO$_x$) for both samples (15 and 55 s) weakly diminishes at higher thermal temperatures [Fig. 2(b)]. These two precedent results are due to the oxidation front during the oxidation process (t_{Ox} and/or T_{Ann}). Concerning the densities, an increase of ρ(AlO$_x$) with T_{Ann} is observed, due to the formation of the alumina layer [with ρ approaching the bulk value, Fig. 3(b)] from the annealing. And maxima of ρ(Co) and ρ(CoO) are obtained for $T_{Ann} = 300$ °C [see Figs. 3(a) and 3(c)]. As a main result, a diminishing of ρ is systematically observed, due to probable poorly densified layers.

By attentively looking at the ratio between the roughness and the associated thickness, the samples can be divided into two groups, depending on the annealing temperatures: (1) For as-grown samples, notable roughness/thickness ratios (rms/Th) are estimated for the following layers: AlO$_x$ (69%), Al (54%), and Co (31%). And for the sample oxidized during 55 s, rms/Th = 29% and 65% for AlO$_x$ and Co, respectively.

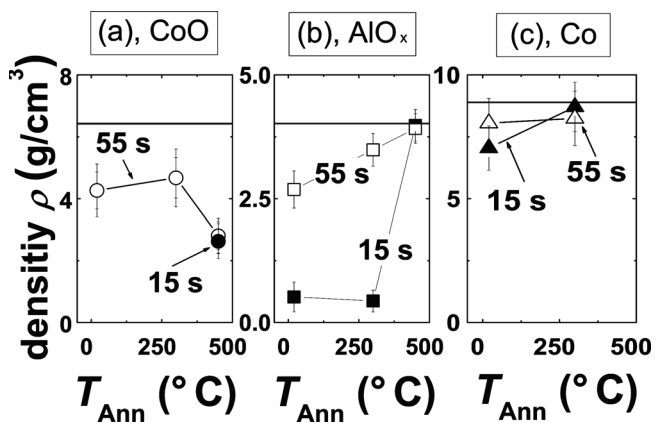

FIG. 3. Mass densities ρ vs T_{Ann} for each layer [CoO (a), AlO$_x$ (b), and Co (c)] of Pt/Co/AlO$_x$ oxidized during 15 and 55 s. Expected bulk values are added in straight lines.

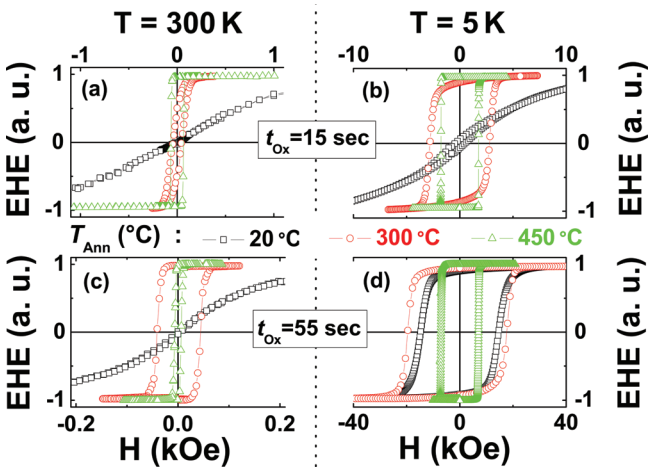

FIG. 4. (Color online) Normalized Hall resistance EHE vs the magnetic field H for Pt/Co/AlO_x oxidized for $t_{Ox} = 15$ s [(a) and (b)], and 55 s [(c) and (d)], and annealed at different T_{Ann}. The measurement temperature $T = 300$ K [(a) and (c)] and $T = 5$ K [(b) and (d)]. Note the different x scale between (a) and (b) and between (c) and (d).

Low densities and weak thicknesses of AlO_x are extracted from the adjustments. (2) For annealed stacks, the rms/Th ratios are lowered: (21–30)%, (25–35)%, and (37–53)% ranges for, respectively, AlO_x, Co, and CoO. In particular, these ratios are minimized at moderate temperature (300 °C) especially for Co and CoO. Also strong densities and maximized thickness of AlO_x are found from the adjustments. Buchanan *et al.*[10] have measured robust as-grown tunnel junctions with remarkable Th(AlO_x) and weak rms(AlO_x) from grazing incidence XRR data and associated fits. These morphological results are crucial for understanding magnetic properties in such trilayers.

Hysteresis loops at 300 and 5 K were carried out by measuring EHE for as-grown Pt/CoO/AlO_x oxidized during 15 and 55 s, and annealed at $T_{Ann} = 300$ and 450 °C (see Fig. 4). As preliminary observed in Ref. 5 at RT [Fig. 4(a)] and 5 K [Fig. 4(b)], for as-grown samples, an in-plane easy axis is predominant at low oxidation time (15 s). Also a noteworthy PMA surprisingly appears for higher t_{Ox} at low T [55 s, Fig. 4(d)]. For this previous sample, an appreciable thickness of AlO_x (~2 nm) and densities of layers are extracted from fits of XRR data. Here, efficient quantities of oxygen at the interface of the Co layer might contribute to an out-of-plane component of the magnetization. Consequently, the samples of the group (1) [low density, weak Th(AlO_x), and strong rms/Th] are corresponding for the large part to an in-plane easy axis. At RT [Figs. 4(a) and 4(c)], the effect of thermal annealing on the EHE response is to induce or reinforce PMA with square loop, low saturation fields, and increased coercive field (H_c). In addition, the more the sample is oxidized (55 compared to 15 s), the higher values of H_c and remanence are recorded. At 5 K, the out-of-plane magnetization persists for both t_{Ox}. Remarkable values of H_c are noted at 5 K for $t_{Ox} = 55$ s: 1.86 and 0.71 T for 300 and 450 °C, respectively. And H_c is moderately increased at 5 K for the sample oxidized for 15 s (0.28–0.18) T for $T_{Ann} = 300$ and 450 °C respectively. The hypothesis for explaining such results lies on the improved interfacial quality between the ferromagnetic layer and the oxide from the annealing process, as mentioned for the samples of the group (2) [density approaching the bulk value, strong Th(AlO_x), and weak rms/Th]. The origin of the strong temperature dependence of magnetic properties could be mainly explained by an antiferromagnetic coupling (see Ref. 11 for MgO/Co bilayers) between Co and CoO entities. Here, no exchange bias fields are observed due to the weak thickness of CoO, as observed in Ref. 12, for tunnel junctions. Finally, Co–Pt bondings are a second reason for the improvement of PMA specially for annealed samples.

In summary, the temperature dependence of Pt/Co/AlO_x, with different oxidation times and annealing temperatures, is well understood by the mean of quantitative analysis of x-ray specular reflectometry. In particular, from our structural approach via the reflectometry technique, the *quality* of the perpendicular magnetic anisotropy in magnetic nanostructures could be tuned by a proper choice of structural deposition parameters (oxidation) as well as the thermal annealing.

[1] I. I. Oleinik, E. Y. Tsymbal, and D. G. Pettifor, Phys. Rev. B **62**, 3952 (2000).
[2] N. Nakajima, T. Koide, T. Shidara, H. Miyauchi, H. Fukutani, A. Fujimori, K. Iio, T. Katayama, M. Nyvlt, and Y. Suzuki, Phys. Rev. Lett. **81**, 5229 (1998).
[3] A. Manchon, S. Pizzini, J. Vogel, V. Uhlir, L. Lombard, C. Ducruet, S. Auffret, B. Rodmacq, B. Dieny, M. Hochstrasser, and G. Panaccione, J. Magn. Magn. Mater. **320**, 1889 (2008).
[4] A. Manchon, S. Pizzini, J. Vogel, V. Uhlir, L. Lombard, C. Ducruet, S. Auffret, B. Rodmacq, B. Dieny, M. Hochstrasser, and G. Panaccione, J. Appl. Phys. **103**, 07A912 (2008).
[5] B. Rodmacq, A. Manchon, C. Ducruet, S. Auffret, and B. Dieny, Phys. Rev. B **79**, 024423 (2009).
[6] F. Fettar, H. Garad, L. Ortega, A. Y. Ramos, B. Zawilski, P. Plaindoux, S. Auffret, B. Rodmacq, and B. Dieny, IEEE Trans. Magn. **45**, 3905 (2009).
[7] J. D. R. Buchanan, T. P. A. Hase, B. K. Tanner, P. J. Chen, L. Gan, C. J. Powell, and W. F. Egelhoff, Jr., Phys. Rev. B **66**, 104427 (2002).
[8] *DIFFRAC PLUS LEPTOS Analytical Software for XRD and XRR* (Bruker Advanced X-Ray Solutions, 2004); A. Ulyanenkov, Appl. Surf. Sci. **253**, 106 (2006).
[9] L. G. Parratt, Phys. Rev. **95**, 359 (1954).
[10] J. D. R. Buchanan, T. P. A. Hase, B. K. Tanner, N. D. Hughes, and R. J. Hicken, Appl. Phys. Lett. **81**, 751 (2002).
[11] Y. Lu, C. Deranlot, A. Vaures, F. Petroff, and J. M. George, J. Appl. Phys. **104**, 073907 (2008).
[12] K. S. Yoon, J. Y. Yang, W. J. Choi, C. O. Kim, J. P. Hong, and H. J. Kim, Phys. Rev. B **69**, 012407 (2004).